

Interplay of the inverse proximity effect and magnetic field in out-of-equilibrium single-electron devices

Shuji Nakamura,^{1,*} Yuri A. Pashkin,² Mathieu Taupin,³ Ville F. Maisi,^{4,5} Ivan M. Khaymovich,^{6,7,†} Alexander S. Mel'nikov,^{7,8} Joonas T. Peltonen,⁴ Jukka P. Pekola,⁴ Yuma Okazaki,¹ Satoshi Kashiwaya,¹ Shiro Kawabata,¹ Andrey S. Vasenko,⁹ Jaw-Shen Tsai,^{10,11} and Nobu-Hisa Kaneko¹

¹*National Institute of Advanced Industrial Science and Technology,
1-1-1 Umezono, Tsukuba, Ibaraki 305-8563, Japan*

²*Department of Physics, Lancaster University, Lancaster LA1 4YB, UK*

³*Institute of Solid State Physics, Vienna University of Technology,
Wiedner Hauptstrasse 8-10, 1040 Vienna, Austria*

⁴*Low Temperature Laboratory, Department of Applied Physics, Aalto University, 00076 Aalto, Finland*

⁵*Center for Quantum Devices, Niels Bohr Institute, University of Copenhagen,
Universitetsparken 5, 2100 Copenhagen Ø, Denmark*

⁶*Max Planck Institute for the Physics of Complex Systems, D-01187 Dresden, Germany*

⁷*Institute for Physics of Microstructures, Russian Academy of Sciences, 603950 Nizhny Novgorod, GSP-105, Russia*

⁸*Lobachevsky State University of Nizhny Novgorod,*

23 Prospekt Gagarina, 603950, Nizhny Novgorod, Russia

⁹*National Research University Higher School of Economics, 101000 Moscow, Russia*

¹⁰*RIKEN Center for Emergent Matter Science, Wako, Saitama 351-0198, Japan*

¹¹*Department of Physics, Tokyo University of Science, Kagurazaka, Tokyo 162-8601, Japan*

(Dated: April 21, 2017)

We show that a weak external magnetic field affects significantly non-equilibrium quasiparticle (QP) distributions under the conditions of the inverse proximity effect, using the single-electron hybrid turnstile as a generic example. Inverse proximity suppresses the superconducting gap in superconducting leads in the vicinity of turnstile junctions, thus trapping hot QPs in this region. An external magnetic field creates additional QP traps in the leads in the form of vortices or regions with a reduced superconducting gap resulting in the release of QPs away from junctions. We present a clear experimental evidence of the interplay of the inverse proximity effect and magnetic field revealing itself in the superconducting gap enhancement and significant improvement of the turnstile characteristics. The observed interplay and its theoretical explanation in the context of QP overheating are important for various superconducting and hybrid nanoelectronic devices, which find applications in quantum computation, photon detection and quantum metrology.

PACS numbers: 85.35.Gv, 74.25.Ha, 74.45.+c, 73.23.Hk

I. INTRODUCTION

Proximity effect induces superconducting correlations in a normal metal, which is in contact with a superconductor. Besides playing an important role in the physics of superconductors [1], it also provides the basis for engineering the symmetry of the induced superconducting pairing in various hybrid structures [2–5]. Its counterpart, the inverse proximity effect, is responsible for the reduction of the superconducting order parameter due to the penetration of normal electrons into the superconductor [6]. Microscopically, both effects can be understood in terms of the Andreev reflection at the interface of a superconductor and a normal metal [7].

The reduction of the superconducting gap caused by the inverse proximity effect creates traps for nonequilibrium quasiparticles (QPs) at the junction with a normal metal, which adversely affect the performance of many

superconducting devices such as various types of photon detectors and bolometers (see, e.g., [8–11]) refrigerators based on normal metal (N) - insulator (I) - superconductor (S) junctions [12], superconducting resonators [13], superconducting qubits [14, 15], and single-electron hybrid turnstiles [16]. Device performance degradation is especially significant for low-resistance devices since the noticeable gap reduction at the SIN junction requires quite transparent interfaces. The problem of QP removal in these devices is usually solved by introducing additional QP traps away from the junction region, either by using normal metal inclusions [17–19] or the local order parameter suppression by an external magnetic field [12–16] or by using an alternative device design immune to QP overheating [20].

In this paper we address an intriguing possibility to diminish the detrimental effect of the QP traps formed in the vicinity of the junctions, by using an external magnetic field which leads to the nontrivial and counterintuitive increase of the superconducting gap in the junction areas. The presence of different trapping mechanisms and resulting redistribution of nonequilibrium QPs between the traps under the magnetic field is a

* shuji.nakamura@aist.go.jp

† ivan.khaymovich@pks.mpg.de

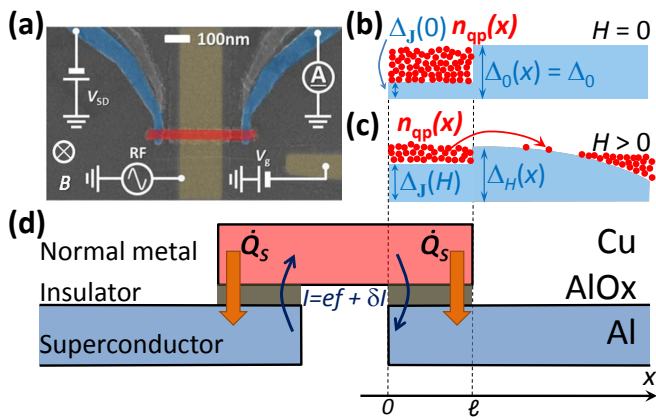


FIG. 1. (a) SEM image of the SINIS turnstile and measurement setup. False color identifies superconducting Al leads (blue), the normal metal Cu island (red), and the DC side gate and RF bottom gate electrodes (both yellow). (b),(c) The gap profile $\Delta_H(x)$ and $\Delta_J = \Delta_H(0)$ (blue shading) and the QP distribution $n_{qp}(x)$ (red circles) in the leads at different magnetic field H values. (d) Schematic cross-section of the structure with charge (blue arrows) and heat (orange arrows) currents. In panels (b) - (d) the overlap junctions are located in the interval $0 < x < \ell$ along x -direction.

rather general phenomenon, which reflects the fundamental properties of superconducting correlations and provides the means to control the gap profile in situ. The inhomogeneous gap profile and its sensitivity to the magnetic field can be used in superconducting and hybrid devices in which superconductors with different gap values are used [8, 9], to tune the gap profile by the applied magnetic field. Indeed, in single-photon detectors one needs to localize QPs generated by high-energy photons in the vicinity of the junction. However, to reduce the time when the detector is overheated and insensitive to subsequent photons, one needs to enhance QP relaxation. Therefore the observed phenomenon of tunability of the gap profile in magnetic field can be straightforwardly utilized in such kind of devices. The magnetic field induced traps (e.g., vortex traps) for the considered gap engineering have also another advantage that is perfect matching of superconducting parts with different gaps without interface mismatch. Apparently, when controlling the position of the magnetic field induced traps (e.g., vortex traps), one should keep the distance from the junction to the nearest vortex to be at least 4 coherence lengths to avoid poisoning of the local density of states there by the low-energy states (see, e.g., [12–16, 21]). Geometry of the superconducting leads is also important for the optimization problem due to its effect on both the quasiparticle diffusion [22] and vortex arrangement.

To observe the interplay between the magnetic field and inverse proximity effect experimentally, we study charge transport through a hybrid turnstile [23], i.e., a single-electron transistor consisting of a normal-metal island with charging energy E_C , tunnel-coupled to voltage-

biased superconducting electrodes (SINIS) and controlled by both DC and RF gate voltages (see Fig. 1(a)). By comparing the samples with different tunnel resistances R_T we clearly demonstrate that the decrease of R_T down to the order of the resistance quantum $R_Q = \frac{h}{e^2} \sim 25.8 \text{ k}\Omega$, enhances the excess current, $\delta I = I - ef$, in the turnstile regime, dominated by the hot QP contribution. Here, the product ef of the elementary electron charge e and the drive frequency f is the ideal value of the current I in the turnstile regime. The decrease of R_T also affects the superconducting gap Δ_J at the junctions, $0 < x < \ell$, keeping the gap $\Delta_0(x) = \Delta_0$ away from the junctions intact, see Fig. 1(b), where x is the coordinate along the leads and ℓ is the size of the proximized region at the SIN junctions (Fig. 1(d)). A weak magnetic field perpendicular to the sample reduces the turnstile excess current and at the same time recovers $\Delta_J(H)$ closer to its bulk value Δ_0 . This is consistent with the developed theoretical model of the release of hot QPs from the vicinity of the junctions due to the reduction of the gap $\Delta_H(x)$ away from the junctions, mediated by the magnetic field (see Fig. 1(c)) leading to the simultaneous gap increase at the junction. This model explains the magnetic-field dependence of the excess current and gives semi-quantitative agreement with the experimental data.

The rest of the paper is organized as follows. In Sec. II we describe some details of the fabrication process and measurement setup and provide information about sample characteristics. The main experimental results on the magnetic field effect on the turnstile operation and on the gap profile are given in Sec. III. Section IV is devoted to the theoretical analysis of the experimental data and discussion. Finally, in Sec. V we sum up our results and give an outlook. Some details of the derivation are given in appendices.

II. FABRICATION, MEASUREMENT SETUP, AND SAMPLE CHARACTERIZATION

The SINIS devices are fabricated on a thermally oxidized Si wafer with the standard electron-beam lithography and metal deposition using angle shadow evaporation technique [24], see scanning electron microscope (SEM) image of one of the samples in Fig. 1(a) and with a smaller magnification in Fig. 6 of Appendix C. Before the final fabrication step in which the SINIS structures were formed, the wafer went through several processing steps to prepare bonding pads and a ground plane. Each chip contains Ti(5 nm)/Au(95 nm) bonding pads and a Ti(5 nm)/Au(50 nm) ground plane that has a slot to accommodate an RF line. The RF line was extended to the center of the chip with a 30 nm-thick and 200 nm-wide Au strip. The whole wafer was then covered by a layer of SiO_2 using spin-on glass which was patterned to open the contact pads. Finally, we fabricate the SINIS turnstiles using a tri-layer resist structure (copolymer resist (400 nm)/Ge(20 nm)/PMMA resist (50 nm)) which

is formed by electron beam lithography and dry etching. SINIS devices are connected to the bonding pads by Al leads stretching from the chip center to the bonding pads above the ground plane, thus a large capacitance is formed between the DC leads and the ground plane protecting sensitive SINIS turnstiles from the electromagnetic noise penetrating into the sample package. Al/AlO_x/Cu tunnel junctions of the SINIS turnstiles are formed by the overlap of the 18 nm-thick Al leads and the 30 nm-thick Cu island deposited in the e-gun evaporator at different angles through a suspended Ge mask formed by electron-beam lithography and dry etching. Aluminum oxide layer on the surface of the deposited Al film is grown by letting pure oxygen or Ar + O₂ mixture into the sample chamber. The tunnel junction resistance is controlled by varying the oxygen/argon pressure and oxidation time.

In this experiment, we use two different setups for oxidation and sample characterization (setup 1 and setup 2). Sample H and sample L are fabricated and measured in setup 1. Aluminum was oxidized under static conditions, when a small amount of gas was introduced into the vacuum chamber. The oxidation conditions are 40 s under 37.5 mTorr of pure oxygen for sample H, and 2 minutes under 97 mTorr Ar + O₂(1 %) for sample L. The measurement is performed in a homemade dilution refrigerator whose base temperature is around 100 mK. The measurement setup used in both setups is shown schematically in Fig. 1(a). The source-drain voltage (V_{SD}) between the superconducting leads is applied using a commercial voltage source (SIM928), a DC gate voltage (V_g) tuning offset charges on the normal-metal island is applied using a commercial voltage source (SIM928), and the current is measured with a room-temperature current amplifier (DDPCA 300 from Femto) calibrated by a standard resistor and a calibrated voltage source in the Metrology Institute of Finland (MIKES). The DC signals (V_{SD} and V_g) are filtered with Thermocoax cables, and the RF line has a -20 dB attenuator at 4.2 K, thermalized in the helium bath, and a -20 dB attenuator at room temperature.

Sample R is fabricated and measured in setup 2. Aluminum was oxidized in a continuous gas flow regime at a constant gas pressure maintained by an automatic pressure regulator. The oxidation condition is 2 minutes under 30 mTorr Ar + O₂(10 %). The measurement is performed in a commercial dilution refrigerator (Oxford Instruments Kelvinox 100) whose base temperature is also about 100 mK. The voltage sources and the current amplifier are same as those in setup 1. Calibration of the current amplifier is done in the Japanese Metrological Institute (AIST). The DC signals (V_{SD} and V_g) are filtered with Thermocoax cables and Cu powder filters, and the RF line has a low pass filter (Mini-Circuits VLFX-1350), a Cu powder filter and a -40 dB attenuator at room temperature.

The sample parameters R_T , E_C , and Δ_0 of the three measured devices listed in Table I have been extracted

TABLE I. Parameters of the measured SINIS turnstiles.

Sample	R_T , k Ω	E_C/Δ_0	Δ_0 , μ eV
H	230	1.6	216
L	55	1.6	215
R	60	1.8	210

Samples H and L are measured in setup 1, while sample R is measured in setup 2. Setup 1 and 2 differ in sample shielding and RF wire filtering.

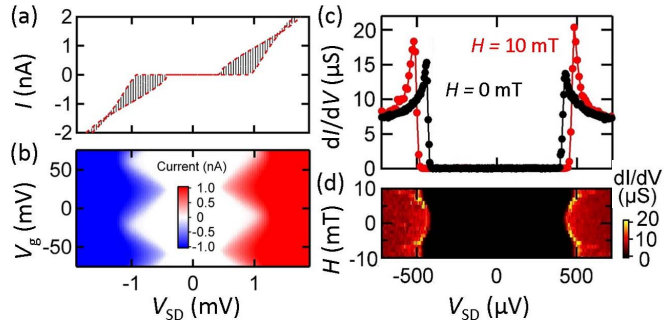


FIG. 2. (a) $I - V$ characteristics of sample H for various dc gate voltages V_g . Dashed red lines are simulated $I - V$ characteristics for the gate-open and closed states; (b) Source-drain turnstile current vs V_g and V_{SD} forming Coulomb blockade diamonds; (c) Differential conductance of sample R as a function of bias voltage at zero (black) and finite (red) magnetic fields H ; (d) Color plot of differential conductance vs V_{SD} and H .

from the $I - V$ characteristics using standard numerical simulation based on the Fermi's golden rule and the master equation [25], see typical $I - V$ curves at different V_g for sample H in Fig. 2(a), (b).

In both setups the normal metal island is capacitively coupled to the RF bottom gate electrode, isolated from the island by the SiO₂ layer. In turnstile experiments, an additional sinusoidal gate voltage with amplitude A_g is applied to this RF gate electrode for the electronic pumping. The pumping experiments are carried out at a drive frequency $f = 100$ MHz with the DC gate voltage V_g fixed at the gate-open state (offset charge of the turnstile island is 0.5) and the source-drain voltage tuned to the optimal point $eV_{SD} = \Delta$ for turnstile operation [23]. The current is measured with a room-temperature current amplifier calibrated by a standard resistor and a calibrated voltage source.

III. TURNSTILE MEASUREMENTS IN MAGNETIC FIELD

At zero magnetic field we observe that the turnstile current for high-resistance sample H with $R_T \sim 9R_Q$ (black dots in Fig. 3(a)) demonstrates back-bending (red dashed line) at high A_g values, in full agreement

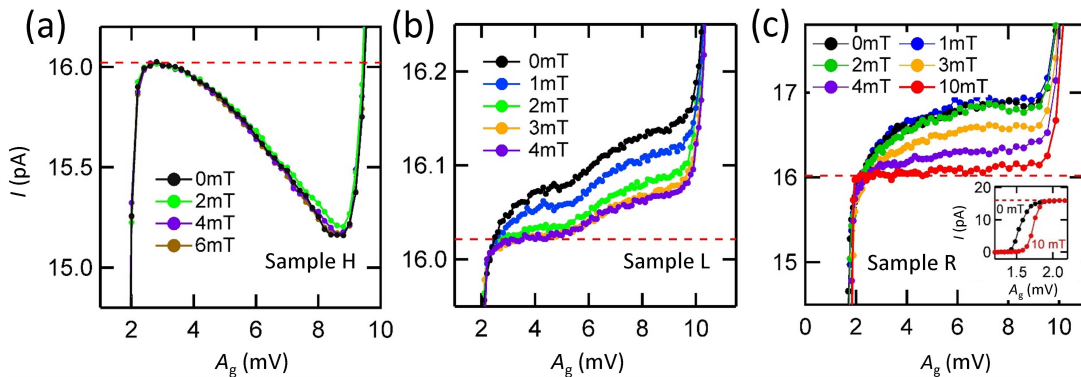


FIG. 3. Pumped current in turnstile regime (colored dots) of (a) sample H, (b) sample L, and (c) sample R vs RF gate amplitude at different magnetic fields. Horizontal red dashed lines show the ideal value of the pumped current $I = ef$ at the turnstile frequency $f = 100$ MHz. (panel c inset) a close-up of the onset of the current plateau at 0 mT and 10 mT.

with the effect of backtunneling processes at high resistance/Coulomb energy [26]. Current I in low-resistance samples L and R (black dots in panels (b) and (c)) with $R_T \sim 2R_Q$ exceeds ef by 0.7 % and 5 %, respectively.

In high-resistance sample H a weak magnetic field applied perpendicular to the substrate has almost no effect on the turnstile current (color dots in Fig. 3(a)), whereas it reduces significantly the excess current in low-resistance samples (color dots in panels (b)–(c)). The observed magnetic-field dependence of the excess current for several gate amplitudes A_g shown by color symbols in Fig. 4 demonstrates this reduction both in Samples L and R. Together with the reduction of the excess current in samples L and R, the RF threshold amplitude value $A_g^{\text{th}} = \Delta_J/e - V_{\text{SD}}/2$ increases (see inset of Fig. 3(c)), even though the dc source-drain and gate voltages are kept unchanged. This points out that superconducting gap Δ_J at the junctions is enhanced by an applied magnetic field [27]. This increment of $\Delta_J(H)$ in the field is observed explicitly by measuring the differential conductance dI/dV in the gate-open state, see plots for sample R in Fig. 2(c), (d). The gap increases by more than 10 % at $H = 10$ mT relative to its zero-field value. The enhancement of the superconducting gap in sample L is qualitatively the same (not shown).

IV. THEORETICAL MODEL AND COMPARISON WITH EXPERIMENTAL DATA

Our quantitative theoretical description is based on the idea schematically shown in Fig. 1(b), (c). At zero field, hot QPs produced due to the turnstile operation are trapped at the junction regions with reduced Δ_J (panel (b)) and cause the excess current [22]. Due to the lead geometry, magnetic field H reduces the gap in the wide region away from the junctions (or even suppresses it due to vortex penetration), opens the way for QPs to escape from the trap and therefore diminishes the overheating of the proximized region (panel (c)). Reduction of both

overheating and the inverse proximity effect enhances the gap Δ_J . Further increase of the field leads to the negative effect on Δ_J diminishing therefore the turnstile accuracy. In the theoretical model we make the following assumptions: (i) The electron-electron relaxation rate is larger than the drive frequency and tunneling rates keeping electronic distributions in the leads to be of the Fermi-Dirac form with effective spatially dependent temperature $T(x)$ [28]; (ii) The excess current $\delta I = I - ef$ is dominated by the overheating contribution (see, e.g., [16, 33, 34])

$$\delta I = C \frac{\sqrt{2\pi\Delta_J k_B T_J}}{eR_T} \exp\left[-\frac{\Delta_J}{k_B T_J}\right] \equiv \frac{C\Delta_J}{eR_T} N_{\text{qp}}(0) \quad (1)$$

with the numerical prefactor $C(A_g) \sim 1$ determined by the wave-form and the amplitude A_g of the RF gate voltage; (iii) In the proximized region, $0 < x < \ell$, the temperature $T(x) = T_J$, the gap $\Delta_J(H, x) = \Delta_J(H)$, and the normalized QP number $N_{\text{qp}}(x)$ are constant [35]; (iv) Most of the dissipated heat $IV_{\text{SD}} \simeq 2\dot{Q}_S$ goes to the leads and keeps N-island close to the equilibrium.

Because the lead width $w(x)$ increases gradually with the distance from the junction, the stationary temperature profile $T(x)$ averaged over $w(x)$ is determined by the solution of the quasi one-dimensional heat diffusion equation

$$\frac{\partial}{\partial x} \left[w(x)\kappa_S(T(x), x) \frac{\partial}{\partial x} T(x) \right] = \dot{q}_{\text{e-ph}}(T(x))w(x) \quad (2)$$

with the following boundary conditions at the junctions, $0 < x < \ell$, $T|_J = T_J$ and away from it, $x \rightarrow \infty$

$$-\kappa_S(T(x), x) \frac{\partial}{\partial x} T(x) \Big|_J = \dot{Q}_S/A, \quad (3a)$$

$$T(x)|_{x \rightarrow \infty} = T_0. \quad (3b)$$

Here T_0 is the phonon bath temperature, $\kappa_S(T(x), x) \sim \frac{2\Delta_H^2(x)}{e^2\rho_n T} e^{-\Delta_H(x)/k_B T}$ is the thermal conductivity of the superconductor, $A \simeq \ell w(0)$ is the junction area, $\rho_n =$

30 nΩm is the normal-state resistivity of the superconductor [22], $\dot{q}_{e-\text{ph}}$ is the density of the heat flux to the phonon bath.

Assuming the conservation of the heat flow and the temperature T_J in the proximized region $0 < x < \ell$ (iii) [36], one can solve Eq. (2) in the region $x > \ell$ with the boundary conditions analogous to Eqs. (3)

$$\kappa_S(T, x) \frac{\partial}{\partial x} T(x) \Big|_{x=\ell+0} = \dot{Q}_\ell / A_\ell, \quad (4a)$$

$$T(x)|_{x=\ell+0} = T(x)|_{x=\ell-0} \equiv T_J. \quad (4b)$$

Here $\dot{Q}_\ell = \dot{Q}_S A_\ell / A \simeq \dot{Q}_S d_S / w(0)$ and $A_\ell = \ell d_S$ are the heat flow rate and the cross-sectional area of the S lead at $x = \ell$.

According to [16, 22] at rather small temperatures $T_0 \ll T \lesssim 0.2\Delta_H(x)/k_B$ the density of the heat flux to the phonon bath can be approximated by the formula $\dot{q}_{e-\text{ph}} \sim \Sigma T^5 e^{-\Delta_H(x)/k_B T}$ neglecting the contributions proportional to $\propto e^{-2\Delta_H(x)/k_B T}$ and $\propto e^{-\Delta_H(x)/k_B T_0}$. Here $\Sigma \simeq 3 \times 10^8 \text{ W K}^{-5} \text{ m}^{-3}$ is the electron-phonon material parameter [37–39].

In this limit the main temperature dependence in both sides of the heat diffusion equation comes from the exponential $e^{-\Delta_H(x)/k_B T}$ and Eq. (1) at $x > \ell$ with logarithmic accuracy in terms of x -dependent QP number $N_{qp}(x)$ takes the form

$$\frac{\partial}{\partial x} \left[w(x) \frac{\partial}{\partial x} \mathcal{N}_{qp}(x) \right] = L_T^{-2} \mathcal{N}_{qp}(x) w(x), \quad (5)$$

with the diffusion coefficient proportional to the width $w(x)$ and the weakly spatially dependent electron-phonon relaxation length $L_T^{-2} = e^2 \rho_n k_B \Sigma T^4(x) / 2\Delta_H(x)$. One can write the solution of this equation for T_J and $N_{qp}(\ell)$ (cf. [22, 40])

$$N_{qp}(\ell) = \sqrt{\frac{2\pi k_B T_J}{\Delta_\ell}} e^{-\frac{\Delta_\ell}{k_B T_J}} \simeq \frac{e^2 \dot{Q}_S \rho_n \mathcal{R}_H[w(x)]}{\ell \sqrt{2k_B T_J} \Delta_\ell^3 / \pi} \quad (6)$$

with the superconducting gap just behind the junctions $\Delta_\ell = \Delta_H(\ell)$ and the geometrical factor $\mathcal{R}_H[w(x)]$ defined as the ratio of the lead resistance normalized to the sheet resistance and being a functional of the lead width $w(x)$.

This normalized resistance $\mathcal{R}_0[w(x)]$ at zero magnetic field is the sum of linear l_k/w_k and logarithmic $\alpha^{-1} \ln(w_{k+1}/w_k)$ terms of one- and two-dimensional Green's functions of the Laplace equation for the k th lead part of the length l_k with constant width $w(x) = w_{k-1}$ and the linearly increasing one $w(x) = w_{k-1} + \delta x_k (w_k - w_{k-1})/l_k$, respectively. Here the coordinate $\delta x_k = x - x_k$ is shifted to be in the range $0 < \delta x_k < l_k$ in the k th lead part and the opening angle is determined by $2 \tan \alpha = (w_k - w_{k-1})/l_k$ (see Appendix B for the details of the sample geometry).

To estimate \mathcal{R}_H at finite magnetic field one should take into account the penetration of vortices into the lead at distances $x > x_c$, where the S leads are already rather

wide to let the first vortex to enter $w(x_c) \sim \sqrt{\Phi_0/\pi H}$ [41]. As the electron-phonon relaxation term in vortices is of the order of the one in the normal metal [16], they simply relax the temperature $T(x) \simeq T_0$ to its phonon bath value T_0 . Therefore, at distances $x > x_c$ one should truncate the summation in \mathcal{R}_H . Note that here we neglect non-local contribution of vortices to the local density of states (LDOS) at the junction taken into account in [16] for the NISIN turnstile with a small superconducting island due to large $x_c > 4\xi$ compared to the coherence length ξ [21].

In the limit of small excess current, $\delta I \ll ef$, one can neglect its contribution to the heat flux rate $\dot{Q}_S \simeq efV_{SD}/2$ and due to the exponential sensitivity of the left-hand side of Eq. (6) to T_J , one can disregard polynomial T_J -dependence in the right-hand side. As a result, using the equality

$$N_{qp}(0) = \sqrt{\frac{2\pi k_B T_J}{\Delta_J}} \left[N_{qp}(\ell) \sqrt{\frac{\Delta_\ell}{2\pi k_B T_J}} \right]^{\Delta_J/\Delta_\ell} \quad (7)$$

with Eq. (6) substituted into it, the excess current normalized to ef (1) can be estimated as follows

$$\frac{\delta I(H)}{ef} \simeq \frac{C \sqrt{2\pi k_B T_J} \Delta_J}{e^2 R_T f} \left[\frac{eV_{SD}}{4\Delta_\ell} \frac{e^2 \rho_n f}{\ell k_B T_J} \mathcal{R}_H \right]^{\Delta_J/\Delta_\ell}. \quad (8)$$

Due to the smallness of the term in the square brackets, the ratio $\Delta_J(H)/\Delta_\ell$ plays a significant role in the magnetic-field dependence of $\delta I/(ef)$. The H -dependence of the terms in brackets is taken into account through the geometrical factor \mathcal{R}_H which varies from $\mathcal{R}_0 \simeq 35$ to $\mathcal{R}_H \simeq 20$ at $H = 10$ mT due to the vortex penetration into the superconducting leads (see Appendix B for details).

The theoretical values of the excess current shown in Fig. 4 are calculated by substituting the self-consistent solution of Eq. (6) for T_J into the general Eq. (1) with the fitting parameters $\Delta_J(0)/\Delta_\ell$ common for all A_g and the amplitude-dependent factor $C(A_g)$, see Appendix A. The gap profile $\Delta_J(H)/\Delta_J(0)$ is taken from the experimental data, see Fig. 2(c), (d). Numerical calculation reproduces the experimental results semi-quantitatively for both samples R and L. The data at the largest amplitude, $A_g = 10$ mV, is fitted with $C(A_g) = 1$. The deviation of the current from the theoretical curves at smaller amplitudes and at larger values of magnetic fields is possibly related to other contributions such as backtunneling, cotunneling, and Andreev processes as the quasiparticle contribution is suppressed. This effect is more significant in sample L (panel (b)) where the excess current is ~ 10 times smaller. An order of magnitude difference in the amplitude and the different A_g -dependence of the excess current in samples R and L with close parameters, see Table I, could be related to the different experimental environment, namely, sample holder shielding and RF wire filtering in setups 1 and 2 causing the different profiles of the actual ac gate voltage applied to the sample.

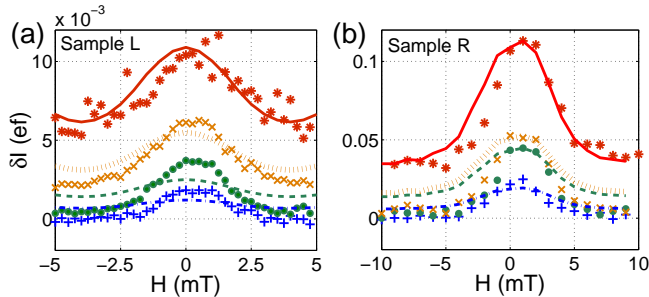


FIG. 4. The excess current $\delta I = I - ef$ normalized to ef through (a) sample L and (b) sample R vs magnetic field at $A_g = 3, 5, 7, 10$ mV (from bottom to top). The experimental data (symbols) is a cross-section of the curves in Fig. 3(b), (c) at fixed A_g . Theoretical curves (lines) are obtained using Eqs. (1, 6). The zero-field gap $\Delta_J(0)/\Delta_0$ at the junctions normalized to its bulk value Δ_0 is fitted as (a) 0.8 and (b) 0.6 for $A_g = 10$ mV (red), the prefactor is taken to be $C = 1$. Other theoretical curves are fitted with respect to $C(A_g)$ with the values: (a) $C = 0.1, 0.2, 0.5, 1$, and (b) $C = 0.17, 0.40, 0.47, 1$ (from bottom to top).

The only subtle point not covered by the developed theoretical model is the 13 % increase of the superconducting gap at the junctions at weak magnetic fields. Instead, the theory takes the magnetic field dependence of the gap from the experimental data and shows its evident relation with the excess current. This gap increase may in principle originate from the enhancement of the order parameter related to the hot quasiparticle density through self-consistency equation. Another possible reason of the increase of $\Delta_J(H)$ is the absence of the H -mediated superfluid velocity in the dead end of the superconducting lead close to the junctions. However, according to the estimates (see Appendix C for details) and to the numerical simulations of the Usadel equation both these effects cannot quantitatively explain the experimentally observed gap variation.

V. CONCLUSIONS

To conclude, we study single-electron pumping in the SINIS turnstile affected simultaneously by the inverse proximity effect and magnetic field. In the samples with a low junction resistance a puzzling magnetic-field dependence of the turnstile current and non-monotonic magnetic-field profile of the superconducting gap at the junctions are observed, while in the high-resistance sample such effects are absent. This puzzle is resolved by the theoretical modeling taking into account both the inverse proximity effect leading to the quasiparticle trapping at the junctions and the overheating of the superconducting leads by hot quasiparticles resulting in the excess current. Perpendicular magnetic field releases hot quasiparticles from the proximized region by suppressing superconduc-

tivity away from the junctions and simultaneously weakening the proximity effect.

Our findings regarding the magnetic-field induced gap increase can be particularly useful for improving the design of cryoelectronic devices suffering from hot quasiparticles. The observed effects of the inhomogeneous spatial gap profile and its tunability by magnetic field have a straightforward application to the devices benefiting from gap engineering, such as single-photon detectors and bolometers [8–11].

ACKNOWLEDGMENTS

We acknowledge fruitful discussions with Yoshitake Takane and Srinivas Gandrothula. This work is partially supported by KAKENHI, Grant Nos. 16H06090 (S.N.) and 15H03525 (Sh. K.), by Academy of Finland, Project Nos. 284594, 272218 (M.T., J.T.P., and J.P.P.), by the UK EPSRC, Grant No. EP/K01675X/1 (Yu.A.P) and the Royal Society, Grant No. WM110105 (Yu.A.P), by the Russian Foundation for Basic Research (I.M.K.), by the Russian Science Foundation, Grant No. 17-12-01383 (A.S.M.), and by the project T3-97 “Macroscopic Quantum Phenomena at Low Temperatures”, carried out within the framework of the Basic Research Program at the National Research University Higher School of Economics (HSE) in 2016 (A.S.V.). We gratefully acknowledge the nanofabrication facilities of the Research Laboratory of NEC Corporation (Tsukuba, Japan) and Otaniemi research infrastructure for Micro and Nanotechnologies (OtaNano, Finland) for the fabrication of the samples.

Appendix A: Quasiparticle dominated excess current

In this section we verify whether the excess current $\delta I = I - ef$ in the turnstile regime of a hybrid single-electron transistor, both of NISIN type with the superconducting island and of SINIS type with the normal metal island, is dominated by the quasiparticle (QP) contribution to the tunneling rates [33, 34].

From the theoretical side as shown in Supplementary Note 6 of [16] the excess current in both types of superconducting hybrid turnstiles takes the form of Eq. (1), where the overheating of S-parts is taken into account by the values of the superconducting gap Δ_J and the electronic temperature T_J at the superconducting side close to the junction with the resistance R_T . A particular form of the numerical coefficient $C(A_g) \sim 1$ considered, e.g., in [16], depends on the wave-form and the amplitude A_g of the RF gate voltage and considered as a fitting parameter of the model.

Other contributions to δI such as Andreev tunneling, cotunneling, and Cooper-pair-electron cotunneling either do not depend on the drive amplitude, or their A_g -dependence cannot be factorized as in Eq. (1).

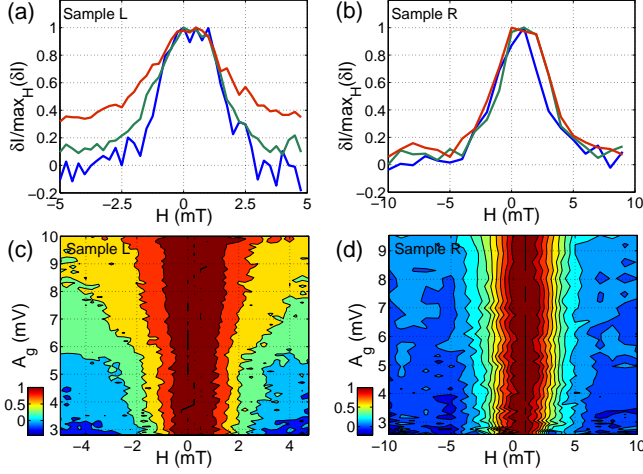


FIG. 5. The excess current $\delta I = I - ef$ in (a, c) sample L and (b, d) sample R normalized to its maximal value versus magnetic field $\max_H(\delta I)$ (a, b) for different amplitude values $A_g = 3$ (blue), 5 (green), and 7 mV (red). Panels (c, d) show color plots of $\delta I / \max_H(\delta I)$ at the turnstile plateau.

Therefore to verify the dominant character of the QP contribution to the excess current experimentally we normalized the magnetic field dependent data $\delta I(H, A_g)$ for different A_g values to its zero field value $\delta I(0, A_g)$, see Fig. 5. The figure shows that in sample R (left panels) the excess current scales with the drive amplitude A_g according to the theoretical factorizing formula (1), i.e., $\delta I(H, A_g) = C(A_g)\delta I_0(H)$. However, in sample L (right panels) where the excess current is ~ 10 times smaller due to additional sample-holder shielding and wire filtering (see Fig. 4(a) in the main text) other contributions play an important role at larger values of magnetic fields as the QP contribution is suppressed. On one hand, this additional shielding leads to the smaller overheating effects (and therefore to the larger gap at the junction $\Delta_J(0)$), but on the other hand, this causes the lower quality of the fitting for sample L as the QP current (1) is not the only contribution to the excess current in this case.

Appendix B: Details of heat diffusion problem

Here we first verify assumption (iii) of the main text and then give the details of the solution of the heat balance equation within the assumptions (i-iv) mentioned in the main text and of the calculation of the normalized resistance $\mathcal{R}_H[w(x)]$ for a certain space profile of the lead width $w(x)$ of the considered samples, see Fig. 6.

Starting with heat diffusion equation (2) with boundary conditions (3), we first consider the proximized region $0 < x < \ell$. As this region is affected homogeneously by the inverse proximity effect we put $\Delta_H(x) = \Delta_J$, i.e., $\kappa_J[T(x)] \sim \frac{2\Delta_J^2}{e^2\rho_n k_B T(x)} e^{-\Delta_J/k_B T(x)}$ and neglect the electron-phonon relaxation \dot{q}_{e-ph} due to the smallness of

the region $\ell \ll L_T$ compared to the electron-phonon relaxation length L_T . This leads to the conservation of the heat flow rate in this region

$$\dot{Q}_\ell = \dot{Q}_S A_\ell / A \simeq \dot{Q}_S d_S / w(0), \quad (B1)$$

where \dot{Q}_ℓ and $A_\ell = \ell d_S$ are the heat flow rate and the cross-sectional area of the S lead at $x = \ell$, the width of the lead in this region is constant $w(0 < x < \ell) = w(0)$. As a result, the heat diffusion equation at $0 < x < \ell$ takes the form

$$\frac{\partial}{\partial x} \left[\kappa_J(T(x)) \frac{\partial}{\partial x} T(x) \right] = 0, \quad (B2)$$

$$-\kappa_J(T(x)) \frac{\partial}{\partial x} T(x) \Big|_{x=0} = \dot{Q}_S / A. \quad (B3)$$

We consider the heat injection to be concentrated at one end $x = 0$, but as we show below the detailed spatial distribution of the heat injection does not matter. Indeed, assuming the constant lead width in the region $x < \ell$, one can find that for $k_B T(x) \ll \Delta_J$ the QP number decays linearly with coordinate

$$\mathcal{N}_{qp} = \sqrt{\frac{2\pi k_B T(x)}{\Delta_J}} e^{-\frac{\Delta_J}{k_B T(x)}} \simeq \mathcal{N}_{qp}(0) - \frac{\dot{Q}_S e^2 \rho_n x}{2A k_B T_J \Delta_J}.$$

In most cases the second term is negligible provided the $x < \ell \ll L_T$, therefore assumption (iii) of the main text $\mathcal{N}_{qp} \simeq \mathcal{N}_{qp}(0)$ and $T(x < \ell) \simeq T_J$ is valid.

In the rest of this section we consider the concrete lead geometry of the measured samples (shown in Fig. 6) and give estimates for the corresponding geometrical factor $\mathcal{R}_H[w(x)]$ used in Eq. (6) and being a functional of the lead width profile. The lead geometry of the considered samples shown in Fig. 1 of the main text and in Fig. 6 leads to the following width profile

$$w(x) = \begin{cases} \ell + \frac{w_1 - \ell}{l_1} \delta x_0, & 0 < \delta x_0 < l_1 \\ w_1 + \frac{w_2 - w_1}{l_2} \delta x_1, & 0 < \delta x_1 < l_2 \\ w_2 + \frac{w_3 - w_2}{l_3} \delta x_2, & 0 < \delta x_2 < l_3 \\ w_3, & 0 < \delta x_3 \end{cases} \quad (B4)$$

where $\delta x_k = x - \ell - \sum_{i=1}^k l_i$ and the junction region $0 < x < \ell$ with $w(x) = \ell$ is followed by a set of linearly opening parts with corresponding lengths l_k and width $w(x)$ changing from w_{k-1} to w_k .

Taking the value estimates from the SEM micrographs $\ell \simeq 50$ nm, $w_1 \simeq 275$ nm, $w_2 \simeq 842$ nm, $w_3 \simeq 8.4$ μ m, $l_1 \simeq 2.85$ μ m, $l_2 \simeq 2.4$ μ m, $l_3 \simeq 28$ μ m and using the estimate $L_T^2 = \frac{R_T \ell^2 d_S}{\rho_n} \sqrt{\frac{2k_B T}{\pi \Delta_\ell}} \simeq (5 \mu\text{m})^2$ from [22] (in the presence of a normal shadow trap lying on top of the S lead far away from the junction with the same sheet NIS resistance) one can obtain at zero magnetic field

$$\mathcal{R}_0 = \sum_{k=1}^3 \frac{l_k}{w_k - w_{k-1}} \ln \left(\frac{w_k}{w_{k-1}} \right) + \frac{L_T}{w_3} \simeq 35. \quad (B5)$$

Taking into account the estimate of \mathcal{R}_H at finite magnetic field given in the main text with the critical width for the first vortex entry $w(x_c) \simeq \sqrt{\Phi_0/\pi H} \simeq 250$ nm for $H \simeq 10$ mT, we keep only the first term in sum in Eq. (B5) with w_1 substituted by $w(x_c)$ in the logarithm. It gives eventually

$$\mathcal{R}_H \approx \frac{l_1}{w_1 - w_0} \ln \left(\frac{w(x_c)}{w_0} \right) \simeq 20. \quad (\text{B6})$$

Appendix C: Estimates of the gap Δ_J variations with H and T_J

According to the experimental data (see Fig. 2(c) of the main text) the gap Δ_J at the junction of Sample R increases by 13 % as the magnetic field increases from 0 to 10 mT [42]. In this section we estimate the influence of a depairing parameter and of QP traps (via the variation of the electronic temperature T_J at the junction) on Δ_J and show that these effects are negligible in the measured experimental setup.

We start with the depairing parameter effect. In the diffusion limit with coherence length $\xi \gg l_{mfp}$ well exceeding the mean free path l_{mfp} one can find the superconducting gap Δ_J in the QP spectrum at a finite magnetic field H as follows (see, e.g., [43–46])

$$\Delta_J = \Delta_S(H)(1 - \gamma_H^{2/3})^{3/2}, \quad (\text{C1})$$

where $\Delta_S(H) = \Delta_0 \exp(-\pi\gamma_H/4)$ is the superconducting order parameter, $\gamma_H = \frac{\hbar\langle v_S^2 \rangle}{2D\Delta_S(H)}$ is the depairing parameter, D_S is the diffusion coefficient in the superconductor, and $\langle v_S^2 \rangle = (\pi DH\ell)^2/3\Phi_0^2$ is the averaged square of the superfluid velocity.

Strictly speaking this analysis works for small widths, $\ell \ll \xi$, of the superconducting leads near the junction, therefore we will use it only for estimates. For experimental parameters $\xi \simeq 100$ nm, $\ell = 50$ nm, $H \simeq 10$ mT, the depairing parameter is rather small

$$\gamma_H = \frac{1}{6} \left(\frac{\pi H \xi \ell}{\Phi_0} \right)^2 \simeq 0.001, \quad (\text{C2})$$

and it leads to a decrease of the superconducting gap by less than 2%

$$1 - \Delta_J(H)/\Delta_0 \simeq 0.016, \quad (\text{C3})$$

which is nearly an order of magnitude smaller than the experimentally observed increase by 5 % and 13 % for samples L and R, respectively.

Now we consider the effect of QP traps on the gap Δ_J . Starting with the experimental data for the excess current $\delta I/(ef)$ shown in Fig. 4 of the main text and taking into account Eq. (1), drive frequency $f = 100$ MHz and junction resistance $R_T \simeq 55 - 60$ k Ω , we estimate the ratio $r(H) = k_B T_J(H)/\Delta_J(H)$ for both samples L and R at $H_0 = 0$ and $H_1 = 10$ mT, see Table II.

TABLE II. Temperature-over-gap ratio.

Sample	$k_B T_J(0)/\Delta_J(0)$	$k_B T_J(H_1)/\Delta_J(H_1)$
L	0.094	0.086
R	0.120	0.095

As the superconducting gap at the junction can be only suppressed comparing to its equilibrium bulk value Δ_0 both by the inverse proximity effect and by the depairing parameter (see estimates above), one can use the ratios mentioned in the Table II as the upper bounds for temperatures $k_B T_J(H) \leq r(H)\Delta_0$. On the other hand, any variations of the electronic temperature $T_J(H)$ (due to the presence of QP traps away from junctions) at such small absolute values ($k_B T_J(H) \leq 0.12\Delta_0$) can only slightly change the self-consistent order parameter value

$$1 - \frac{\Delta_S(H, T_J(H))}{\Delta_0} \simeq \sqrt{\frac{2\pi k_B T_J(H)}{\Delta_S(H)}} e^{-\frac{\Delta_S(H)}{k_B T_J(H)}} \lesssim \frac{e R_T \delta I}{\Delta_0} < 2 \cdot 10^{-4}. \quad (\text{C4})$$

Here we used the maximal value of $\delta I/(ef) \simeq 0.12$ for sample R on the plateau.

We also performed numerical calculations of LDOS by solving Usadel equation together with the self-consistency equation for a superconducting order parameter in a quasi-one-dimensional approximation of the leads near the junction and in the overlap geometry of an NIS tunnel contact used in the experiments (see Fig. 1(a) of the main text). We do not present the results of these numerical simulations here as it has been shown that both the negative effect of depairing parameter and the stimulating effect of QP traps are in quantitative agreement with simple estimates mentioned above and cannot explain the experimentally observed increase of the superconducting gap in a weak magnetic field.

[1] P. G. de Gennes, *Superconductivity of Metals and Alloys* (Addison-Wesley, New York, 1989).
 [2] V. Mourik, K. Zuo, S. M. Frolov, S. R. Plissard, E. P. A.

M. Bakker, and L. P. Kouwenhoven, Signatures of Majorana fermions in hybrid superconductor-semiconductor nanowire devices, *Science* **336**, 1003 (2012).

- [3] M. Eschrig and T. Löfwander, Triplet supercurrents in clean and disordered half-metallic ferromagnets, *Nat. Phys.* **4**, 138 (2008).
- [4] F. Giazotto, J. T. Peltonen, M. Meschke, and J. P. Pekola, Superconducting quantum interference proximity transistor, *Nat. Phys.* **6**, 254 (2010).
- [5] A. Ronzani, C. Altimiras, F. Giazotto, Highly sensitive superconducting quantum-interference proximity transistor, *Phys. Rev. Appl.* **2**, 024005 (2014).
- [6] P. G. D. Gennes, Boundary effects in superconductors, *Rev. Mod. Phys.* **36**, 225 (1964).
- [7] M. Tinkham, *Introduction to superconductivity*, 2nd ed. (Dover Publications, 2004).
- [8] A. A. Golubov and E. P. Houwman, Quasiparticle relaxation rates in a spatially inhomogeneous superconductor, *Physica C* **205**, 147 (1993).
- [9] A. A. Golubov, E. P. Houwman, J. G. Gijsbertsen, J. Flokstra, H. Rogalla, J. B. le Grand, and P. A. J. de Korte, Quasiparticle lifetimes and tunneling times in a superconductor-insulator-superconductor tunnel junction with spatially inhomogeneous electrodes. *Phys. Rev. B* **49**, 12953 (1994).
- [10] G. N. Goltsman, O. Okunev, G. Chulkova, A. Lipatov, A. Semenov, K. Smirnov, B. Voronov, and A. Dzardanov, Picosecond superconducting single-photon optical detector, *Appl. Phys. Lett.* **79**, 705 (2001).
- [11] P. L. Richards, Bolometers for infrared and millimeter waves, *J. Appl. Phys.* **76**, 1 (1994).
- [12] J. T. Peltonen, J. T. Muhonen, M. Meschke, N. B. Kopnin and J. P. Pekola, Magnetic-field-induced stabilization of nonequilibrium superconductivity in a normal-metal/insulator/superconductor junction, *Phys. Rev. B* **84**, 220502(R) (2011).
- [13] I. Nsanzineza and B. L. T. Plourde, Trapping a single vortex and reducing quasiparticles in a superconducting resonator, *Phys. Rev. Lett.* **113**, 117002 (2014).
- [14] C. Wang, Y. Y. Gao, I. M. Pop, U. Vool, C. Axline, T. Brecht, R. W. Heeres, L. Frunzio, M. H. Devoret, G. Catelani, L. I. Glazman and R. J. Schoelkopf, Measurement and control of quasiparticle dynamics in a superconducting qubit, *Nat. Comm.* **5**, 5836 (2014).
- [15] U. Vool, I. M. Pop, K. Sliwa, B. Abdo, C. Wang, T. Brecht, Y. Y. Gao, S. Shankar, M. Hatridge, G. Catelani, M. Mirrahimi, L. Frunzio, R. J. Schoelkopf, L. I. Glazman, and M. H. Devoret, Non-Poissonian quantum jumps of a fluxonium qubit due to quasiparticle excitations, *Phys. Rev. Lett.* **113**, 247001 (2014).
- [16] M. Taupin, I. M. Khaymovich, M. Meschke, A. S. Mel'nikov, J. P. Pekola, Tunable quasiparticle trapping in Meissner and vortex states of mesoscopic superconductors, *Nat. Comm.* **7**, 10977 (2016).
- [17] D. J. Goldie, N. E. Booth, C. Patel, G. L. Salmon, Quasiparticle trapping from a single-crystal superconductor into a normal-metal film via the proximity effect, *Phys. Rev. Lett.* **64**, 954 (1990).
- [18] J. N. Ullom, P. A. Fisher, M. Nahum, Measurements of quasiparticle thermalization in a normal metal, *Phys. Rev. B* **61**, 14839 (2000).
- [19] S. Rajauria, L. M. A. Pascal, Ph. Gandit, F. W. J. Hekking, B. Pannetier, H. Courtois, Efficiency of quasiparticle evacuation in superconducting devices, *Phys. Rev. B* **85**, 020505(R) (2012).
- [20] D. M. T. van Zanten, D. M. Basko, I. M. Khaymovich, J. P. Pekola, H. Courtois, C. B. Winkelmann, Single quantum level electron turnstile, *Phys. Rev. Lett.* **116**, 166801 (2016).
- [21] J. T. Peltonen, P. Virtanen, M. Meschke, J. V. Koski, T. T. Heikkilä, and J. P. Pekola Thermal conductance by the inverse proximity effect in a superconductor, *Phys. Rev. Lett.* **105**, 097004 (2010).
- [22] H. S. Knowles, V. F. Maisi, and J. P. Pekola, Probing quasiparticle excitations in a hybrid single electron transistor, *Appl. Phys. Lett.* **100**, 262601 (2012).
- [23] J. P. Pekola, J. J. Vartiainen, M. Möttönen, O.-P. Saira, M. Meschke, and D. V. Averin, Hybrid single-electron transistor as a source of quantized electric current, *Nat. Phys.* **4**, 120 (2007).
- [24] T. A. Fulton and G. J. Dolan, Observation of single-electron charging effects in small tunnel junctions, *Phys. Rev. Lett.* **59**, 109 (1987).
- [25] A. Kemppinen, M. Meschke, M. Möttönen, D.V. Averin, and J.P. Pekola, Quantized current of a hybrid single-electron transistor with superconducting leads and a normal-metal island, *Eur. Phys. J. Special Topics* **172**, 311 (2009).
- [26] A. Kemppinen, S. Kafanov, Y. A. Pashkin, J. S. Tsai, D. V. Averin, and J. P. Pekola, Experimental investigation of hybrid single-electron turnstiles with high charging energy, *Appl. Phys. Lett.* **94**, 172108 (2009).
- [27] The similar effect of the increase of a threshold in NIS cooler associated with the superconducting gap has been observed in [12].
- [28] Here we consider only quasiequilibrium regime with Fermi-Dirac electron distribution function $f(E)$ in contrast to several works [29–32] considering general form of $f(E)$ both in the superconducting and normal parts.
- [29] J. P. Pekola, T. T. Heikkilä, A. M. Savin, J. T. Flyktman, F. Giazotto, F. W. J. Hekking, Limitations in cooling electrons by normal metal - superconductor tunnel junctions, *Phys. Rev. Lett.* **92**, 056804 (2004).
- [30] F. Giazotto, T. T. Heikkilä, F. Taddei, Rosario Fazio, J. P. Pekola, F. Beltram, Tailoring Josephson coupling through superconductivity-induced nonequilibrium, *Phys. Rev. Lett.* **92**, 137001 (2004).
- [31] M. A. Laakso, P. Virtanen, F. Giazotto, and T. T. Heikkilä, Nonequilibrium characteristics in all-superconducting tunnel structures, *Phys. Rev. B* **75**, 094507 (2007).
- [32] I. M. Khaymovich and D. M. Basko, Recovery of SINIS turnstile accuracy in a strongly nonequilibrium regime, *Phys. Rev. B* **94**, 165158 (2016).
- [33] O.-P. Saira, A. Kemppinen, V. F. Maisi, and J. P. Pekola, Vanishing quasiparticle density in a hybrid Al/Cu/Al single-electron transistor, *Phys. Rev. B* **85**, 012504 (2012).
- [34] V. F. Maisi, Improving the performance of a single-electron turnstile, PhD Thesis, Aalto University (2014).
- [35] This is valid due to homogeneity of the heat inflow and the smallness of ℓ with respect to the electron-phonon relaxation length L_T .
- [36] This assumption is verified in Appendix B.
- [37] R. L. Kautz, G. Zimmerli, and J. M. Martinis, Self-heating in the Coulomb-blockade electrometer, *J. Appl. Phys.* **73**, 2386 (1993).
- [38] F. Giazotto, T. T. Heikkilä, A. Luukanen, A. M. Savin, and J. P. Pekola, Opportunities for mesoscopics in thermometry and refrigeration: Physics and applications, *Rev. Mod. Phys.* **78**, 217 (2009).

- [39] V. F. Maisi, S. V. Lotkhov, A. Kemppinen, A. Heimes, J. T. Muhonen, and J. P. Pekola, Excitation of single quasiparticles in a small superconducting Al island connected to normal-metal leads by tunnel junctions, *Phys. Rev. Lett.* **111**, 147001 (2013).
- [40] S. Rajauria, H. Courtois, and B. Pannetier, Quasiparticle-diffusion-based heating in superconductor tunneling microcoolers, *Phys. Rev. B* **80**, 214521 (2009).
- [41] G. Stan, S. B. Field, J. M. Martinis, Critical field for complete vortex expulsion from narrow superconducting strips, *Phys. Rev. Lett.* **92**, 097003 (2004).
- [42] The corresponding increase of the gap at the junction of Sample L is $\sim 5\%$.
- [43] S. Skalski, O. Betbeder-Matibet, and P. R. Weiss, Properties of superconducting alloys containing paramagnetic impurities, *Phys. Rev.* **136**, A1500-A1518 (1964).
- [44] P. Fulde, Tunneling density of states for a superconductor carrying a current, *Phys. Rev.* **137**, A783-A787 (1965).
- [45] K. Maki, and P. Fulde, Equivalence of different pair-breaking mechanisms in superconductors, *Phys. Rev.* **140**, A1586-A1592 (1965).
- [46] A. Anthore, H. Pothier, and D. Esteve, Density of states in a superconductor carrying a supercurrent, *Phys. Rev. Lett.* **90**, 127001 (2003).

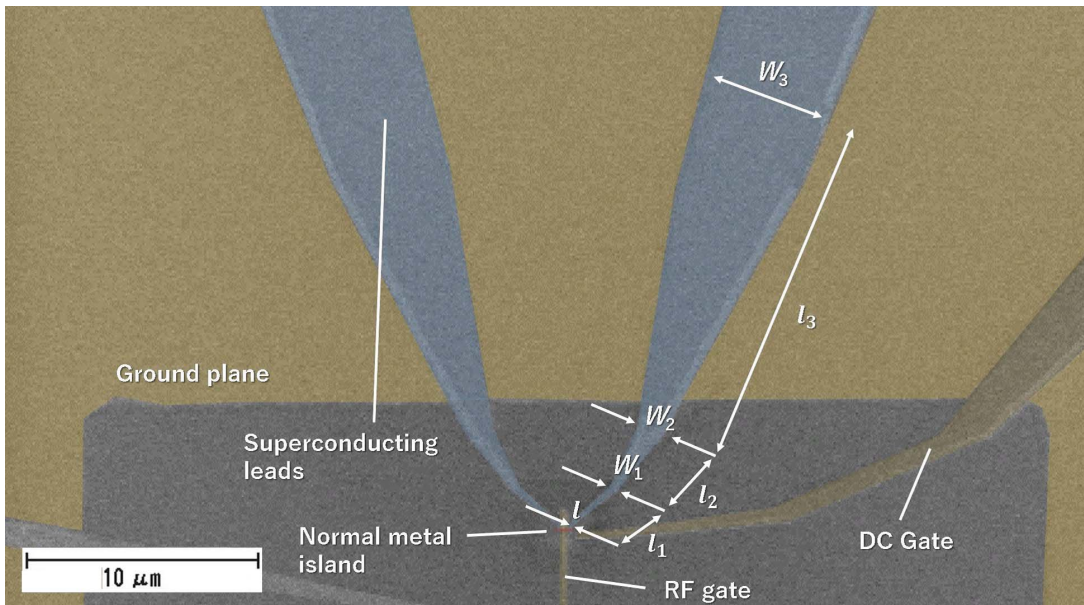


FIG. 6. SEM image of the SINIS single-electron transistor shown in Fig. 1(a) of the main text at larger spatial scale. As in the main text false color identifies superconducting Al leads (blue), the normal metal Cu island (red), and the ground plane as well as the DC side gate and RF bottom gate electrodes (all yellow). Widths l , w_k and lengths l_k mentioned in Eq. (B4) are shown in the figure.